Tangentially Migrating Neurons Assemble a Primary Cilium that Promotes Their Reorientation to the Cortical Plate

Jean-Pierre Baudoin,[1,2,7] Lucie Viou,[1,2,7] Pierre-Serge Launay,[1,2] Camilla Luccardini,[1,2] Sergio Espeso Gil,[1,2] Vera Kiyasova,[1,2] Théano Irinopoulou,[1,2] Chantal Alvarez,[1,2] Jean-Paul Rio,[1,2] Thomas Boudier,[3,4] Jean-Pierre Lechaire,[3,4] Nicoletta Kessaris,[5] Nathalie Spassky,[6] and Christine Métin[1,2,*]

[1]INSERM, UMRS-839, Institut du Fer à Moulin, 17 rue du Fer à Moulin, 75005 Paris, France
[2]Université Pierre et Marie Curie, 17, rue du Fer à Moulin, 75005 Paris, France
[3]IFR83, 7 quai St Bernard, 75005 Paris, France
[4]Université Pierre et Marie Curie, 4 place Jussieu, 75005 Paris, France
[5]Wolfson Institute for Biomedical Research and Department of Cell and Developmental Biology, University College London, Gower Street, London WC1E 6BT, UK
[6]Institut de Biologie de l'Ecole Normale Supérieure, 46, rue d'Ulm, F-75230 Paris cedex 05, Paris
[7]These authors contributed equally to this work
*Correspondence: christine.metin@inserm.fr
http://dx.doi.org/10.1016/j.neuron.2012.10.027

SUMMARY

In migrating neurons, the centrosome nucleates and anchors a polarized network of microtubules that directs organelle movements. We report here that the mother centriole of neurons migrating tangentially from the medial ganglionic eminence (MGE) assembles a short primary cilium and exposes this cilium to the cell surface by docking to the plasma membrane in the leading process. Primary cilia are built by intraflagellar transport (IFT), which is also required for Sonic hedgehog (Shh) signal transduction in vertebrates. We show that Shh pathway perturbations influenced the leading process morphology and dynamics of MGE cells. Whereas Shh favored the exit of MGE cells away from their tangential migratory paths in the developing cortex, cyclopamine or invalidation of IFT genes maintained MGE cells in the tangential paths. Our findings show that signals transmitted through the primary cilium promote the escape of future GABAergic interneurons from their tangential routes to colonize the cortical plate.

INTRODUCTION

Neuronal migration is a directional process achieved by periodic translocation of the cell body within a long thin exploring process. We and others have described two main steps in the cell body translocation (Solecki et al., 2004; Bellion et al., 2005; Schaar and McConnell, 2005; Tsai et al., 2007): first, the endomembrane system (endoplasmic reticulum, ER, and Golgi apparatus, GA) and the centrosome (CTR) move forward during a resting phase of the nucleus, and second the nucleus trans-

locates to the rostral cytoplasmic swelling comprising the CTR/GA complex. The CTR is a microtubule-organizing center (MTOC) that usually lies between the leading edge and nucleus of cells showing directed migration (Rakic, 1972; Ueda et al., 1997). In migrating neurons, the CTR is located at the base of the leading neurite and anchors an array of microtubules (MTs)—the so-called perinuclear cage- that binds the nucleus and CTR and directs nuclear movements toward the CTR (Rivas and Hatten, 1995; Higginbotham and Gleeson, 2007). However, the nucleus can precede or transiently overtake the CTR in migrating neurons (Umeshima et al., 2007; Distel et al., 2010), showing that the control of cell directionality is an integrated and complex process that moreover requires MT stability (Baudoin et al., 2008).

An important function of the CTR, which has recently been re-emphasized, is the capacity to differentiate a primary cilium (Christensen et al., 2008; Louvi and Grove, 2011). The primary cilium is a small protrusion at the cell surface assembled and maintained at the distal end of the mother centriole by the intraflagellar transport (IFT) machinery (Rosenbaum and Witman, 2002). The primary cilium functions as an antenna to probe and integrate extracellular signals, especially morphogens and growth factors, to control cell proliferation, cell differentiation, and cell migration (Breunig et al., 2008; Han et al., 2008; Spassky et al., 2008; Schneider et al., 2010). Primary cilia are present in interphasic neural stem cells in embryonic and adult brain as well as in adult differentiated neurons (Cohen et al., 1988; Fuchs and Schwark, 2004; Arellano et al., 2012). Mutations of IFT proteins compromise primary cilium assembly and are associated with pleiotropic disorders including mental retardation and ataxia in humans (Lee and Gleeson, 2010). Although studies in animal models confirm that IFT plays important roles in brain neurogenesis and morphogenesis through impaired Shh signaling (Breunig et al., 2008; Han et al., 2008; Spassky et al., 2008; Willaredt et al., 2008; Gorivodsky et al., 2009; Stottmann et al., 2009; Besse et al., 2011), the role of IFT in controlling neuronal migration is unknown. Whether immature neurons have

a functional primary cilium is uncertain (Louvi and Grove, 2011; Arellano et al., 2012). We have examined this issue in neurons migrating tangentially from the medial ganglionic eminence (MGE) of the basal telencephalon to the cerebral cortex in which they differentiate as cortical GABAergic interneurons. MGE cells first migrate tangentially to the brain surface in the cortical primordium either in the marginal zone or deep in the intermediate zone. Then they colonize the cortical plate (CP) by reorienting their trajectories from tangential to radial or oblique (Tanaka et al., 2003; Yokota et al., 2007). MGE cells successively encounter and interact with different cell types, in contrast to the principal radially migrating cortical neurons that follow a unique support, the radial glia fiber.

In the present study, we analyzed the dynamic behavior of the CTR in migrating MGE cells. Four-dimensional (4D) reconstructions revealed putative contacts between the centrioles and the cell surface. Electron tomography analysis of the centrosomal region in fixed MGE cells showed that the mother centriole could attach to the plasma membrane by a short primary cilium, in particular when located at a long distance in front of the nucleus. Once the mother centriole was anchored to the plasma membrane, centrosomal MTs were positioned on one side of the leading process. We next asked whether a signal originating at the primary cilium could influence MGE cell migration. MGE cells invalidated for *Kif3a* that encodes a subunit of the molecular motor which drives anterograde IFT required for Shh signal transduction (Rosenbaum and Witman, 2002; Han et al., 2008) showed abnormal distributions in vivo, especially in the tangential migratory streams of the developing cortex. Time-lapse video microscopy recording revealed that invalidation of *Kif3a* or *Ift88*, another gene required for anterograde IFT in primary cilium (Haycraft et al., 2007), prevented MGE cells from leaving the deep tangential migratory stream to colonize the CP. This defect was mimicked by cyclopamine treatment and associated to increased clustering of MGE cells whose leading processes oriented parallel to each other. In contrast, Shh promoted CP colonization. Altogether, these results suggest that Shh signals transmitted through the primary cilium of MGE cells favor directional changes necessary for their ultimate targeting to the cerebral cortex.

RESULTS

The Mother Centriole of Tangentially Migrating MGE Cells Docks to the Plasma Membrane by a Short Primary Cilium

By correlating observations in fixed preparations and live cell recording, we had previously proposed a sequence of centrosomal movements associated to the migratory cycle of MGE cells (Bellion et al., 2005; Métin et al., 2008). Here, we analyzed the dynamic behavior of the centrioles in MGE cells migrating on dissociated cortical cells (Figures 1A–1C and see Figures S1A and S1B available online). MGE cells coexpressed GFP that filled the whole cell body and the PACT domain of pericentrin fused to the mKO1 fluorophore (Konno et al., 2008). As expected, in a majority of recorded MGE cells (66%, n = 33), the CTR first moved far away from the stationary nucleus and then the nucleus quickly translocated near the CTR (Figure 1A). Interestingly, 4D

(x, y, z, time) reconstructions and modeling of cell and centriole shapes showed that the CTR transiently reached the MGE cell surface during forward migration (Figure S1B and Figure 1B). Putative contacts were not correlated with CTR stabilization (stars in Figure 1C) suggesting that membrane-bound centrioles still moved forward.

We further investigated the relationships between the centrioles and the plasma membrane by electron microscopy observations in the centrosomal region of MGE cells at different stage of the migration cycle. MGE cells migrating on cortical axons were sectioned parallel to the plane of migration (Figures 1D1 and 1D2). Semithin sections comprising both the CTR and the nucleus were analyzed using high-resolution electron tomography (Koster et al., 1997). In a large proportion of cells with long nucleus to CTR distances the mother centriole identified by the presence of lateral and/or distal appendages was associated to the plasma membrane by its distal end (Figures 1E–1F2 and 1L; 21 cells out of 33). A third of these cells had a short primary cilium that protruded from the mother centriole into the extracellular space. This primary cilium contained an axoneme (Figures 1F1 and 1F2 and Movie S1) and was often less than 500 nm in length, shorter than the primary cilium found on fully differentiated neurons of adult brains (Fuchs and Schwark, 2004; Arellano et al., 2012). The plasma membrane around the primary cilium often formed a thickened asymmetric depression (Figure 1F1).

The Primary Cilium Assembles in a Golgi-Derived Vesicle

Mother centrioles located in the leading process often associated with the plasma membrane. In contrast, centriole pairs located in the perinuclear compartment positioned deep within the cytoplasm (Figures 1G–1I, 1L, S1C, and S1D). There, the mother centriole associated with a large distal vesicle, either round or flattened (Figures 1H and 1I and Movie S2). A short axoneme could protrude from the mother centriole within the vesicle lumen (Figure 1I, black arrow heads). The single large vesicle was sometimes replaced by a row of small vesicles attached to the tip of mother centriole distal appendages (Figure S1D). Pioneer studies (Sorokin, 1962; Cohen et al., 1988) already reported that the ciliogenesis likely starts with the assembly of a centriolar vesicle into which the axoneme elongates. The centriolar vesicle of MGE cells could engulf smaller vesicles (Figure 1H and Movie S2), attesting to vesicular trafficking toward the centriolar vesicle. Accordingly, we noticed a continuum of small vesicles between the neighboring Golgi cisternae and the large centriolar vesicle (Figure 1I, white arrow heads). To obtain further insight into ciliogenesis related vesicular trafficking in migrating MGE cells, we examined the distribution of GMAP-210, a *cis*-Golgi protein that traffics toward the basal body in ciliated cells (Ríos et al., 2004) and that associates with IFT20 (Follit et al., 2008), a component of anterograde IFT particles. The *cis*-GA, as decorated by GMAP-210 antibodies, extended to the CTR, which was not the case for the median GA (Figures 1J and S1E1–S1E3). A GMAP-210 positive Golgi compartment remained associated to the CTR after brefeldin treatment that redistributed the Golgi to the ER but not after MT destabilization
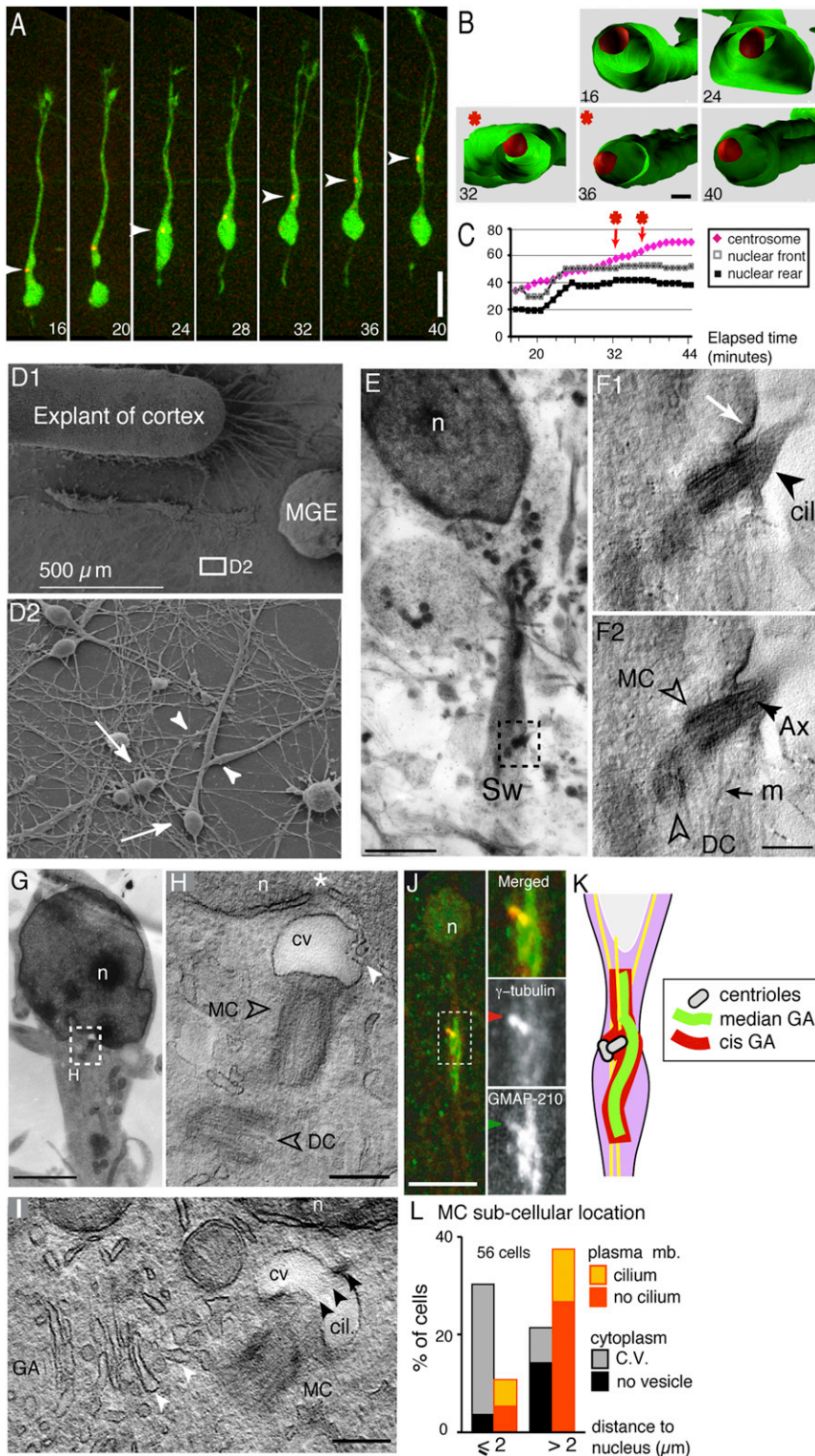
Figure 1. The Mother Centriole of Migrating MGE Cells Associates with a Primary Cilium and Docks to the Plasma Membrane in the Leading Process

(A–C) The centrosome (CTR, red) positions alternatively close to the cell surface in the leading process and deeper in the perinuclear compartment during the migration cycle. A illustrates the sequence of migration of a MGE cell coexpressing EGFP (green) and the centrosomal marker PACT-mKO1 (red). Elapsed time on frames is in minutes. In (B), panels show frontal sections through a 4D model of the cell at the level of the CTR (white arrowheads in A). Curves in (C) represent instantaneous displacements of the CTR (pink), nuclear front (gray), and nuclear rear (black). Putative contacts of the CTR with the plasma membrane are indicated by red stars in (B) and (C). Scale bar in (A), 10 μm; (B), 1 μm.

(D1–I) Subcellular localization of centrioles in migrating MGE cells. Scanning electron micrograph in (D1) and enlarged view in (D2) show MGE cells migrating on cortical axons with recognizable nuclear compartment (D2, arrows) and cytoplasmic swelling (D2, arrow heads). (E) and (G) are low-magnification views of transmission electron micrographs of MGE cells with either long (E) or short (G) nucleus to CTR distance. Dotted squares localize the centrosome analyzed by electron tomography and illustrated by slices from 3D reconstructions in (F1 and F2) and (H), respectively. (I) is a slice from an additional 3D reconstruction. In (E–F2), the mother centriole (MC) docks to the plasma membrane by its distal end in a differentiated region (F1, white arrow) and associates with a short primary cilium (cil.). The MC and daughter centriole (DC) anchor MTs (m). In (G–I), the MC associates by its distal end with a large centriolar vesicle (CV) in which a primary cilium can form (I). Numerous vesicles distribute between the Golgi apparatus (GA) and the CV (I, white arrowheads). Small vesicles can fuse to the large CV (H, white arrowhead). Ax, axoneme; n, nucleus; white star, nuclear pore. Scale bars in (E) and (G), 2 μm; (F2), (H), and (I), 200 nm.

(J) A cis-Golgi compartment immunopositive for GMAP-210 (green) colocalizes with the CTR labeled with γ-tubulin antibodies (red). Enlarged views of the centrosomal region (dotted rectangle) are shown at right. Scale bar, 10 μm.

(K) An interpretative scheme of cis- and median GA labeling in migrating MGE cells.

(L) Quantification of CTR subcellular localization in migrating MGE cells. The MC most often docks to the plasma membrane (red/orange bar) when located more than 2 μm away from the nucleus. When located closer to the nucleus (less than 2 μm), the MC preferentially positions in the cytoplasm (black/gray bar; distributions significantly different by Khi2 test, p < 0.01) and associates with a CV. See also Figure S1, Movie S1, and Movie S2.

(Figures S1F1–S1G2). GMAP-210 thus identified a cis-GA compartment tightly associated with the CTR in a MT dependent manner (see scheme in Figure 1K). The primary cilium of MGE cells likely assembles in a Golgi-derived vesicular compartment associated with the mother centriole by the intermediate of MTs. This Golgi-derived vesicle should fuse to the plasma membrane (Sorokin, 1962; Cohen et al., 1988) to position the primary cilium at the cell surface.
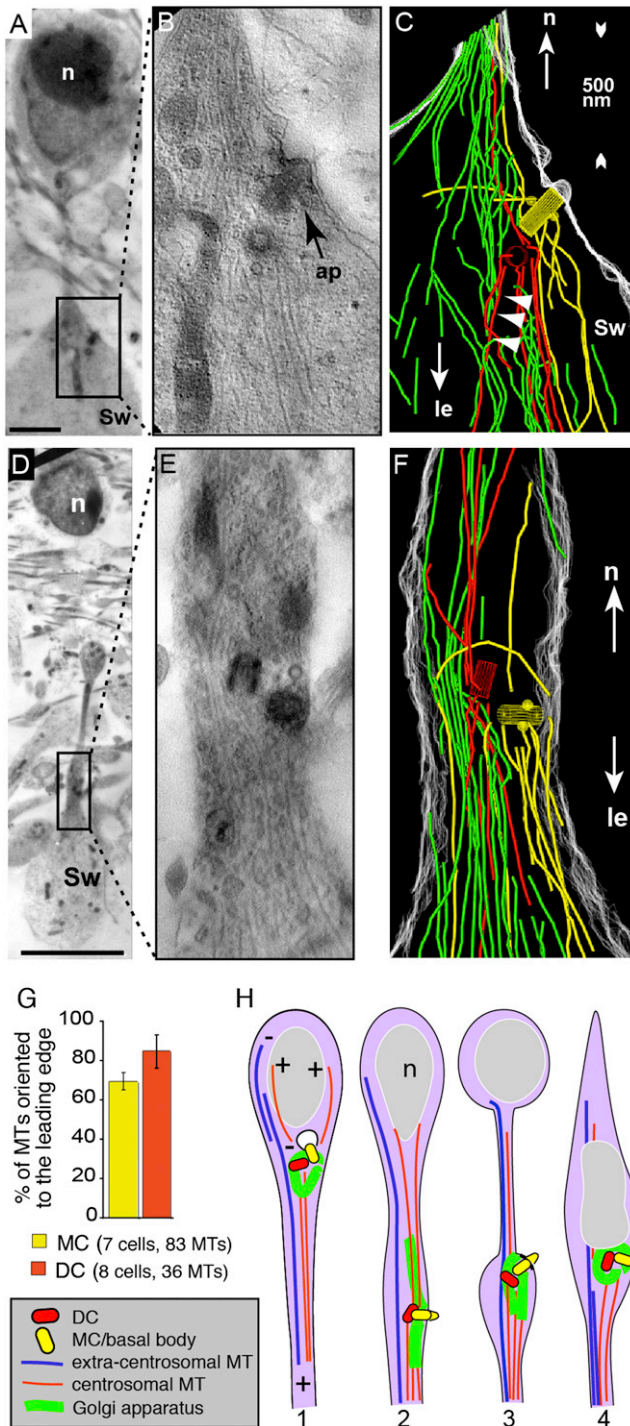
Figure 2. Centrosomal and Extracentrosomal MTs in Migrating MGE Cells with Long Nuclear-Centrosomal Distance

(A–F) Electron tomography analysis of MT organization in the centrosomal region. Rectangles in transmission electron micrographs of semithin sections (A and D) indicate regions reconstructed by electron tomography and illustrated by slices from 3D reconstructions (B and E). Models of 3D reconstructions are shown in (C) and (F). The MC and DC are represented as yellow and red cylinders, respectively. When MTs end less than 50 nm from a centriole, they take the same color as the centriole. Green MTs pass along

The CTR Anchors a Variable Subset of MTs

The CTR nucleates and anchors MTs (Bornens, 2012). The number of centrosomal MTs anchored to the centrioles was significantly higher when the mother centriole was attached to the plasma membrane rather than positioned within the perinuclear cytoplasm (17.7 ± 1.5 anchored MTs against 5.5 ± 1.1, $p < 0.001$, n = 15 cells; compare Figures 1H and 1I and Figure 2B). In similar cocultures prepared for immunostaining, the MT minus-end protein ninein (Baird et al., 2004; Bellion et al., 2005) was detected at the CTR in only a fraction of migrating MGE cells (39%; Figure S2A), attesting that the number of MTs attached to the CTR varied during the migration cycle. A large proportion of MTs reconstructed in the centrosomal region passed alongside the two centrioles without interruption in their vicinity (Figures 2A–2F; $80\% \pm 7.6\%$ of the 87 MTs reconstructed at the rear of the centriole pair in 5 cells; see Movie S3). Thus, a number of MTs does not attach to any centriole in MGE cells, in agreement with γ-tubulin immunostaining that identified the nuclear rear and the rostral swelling as extra-centrosomal sites of MT nucleation (Figure S2B). Since MTs anchored on the centrioles were oriented in majority to the leading edge (Figure 2G), nuclear translocations likely proceed by forward movements along MT bundles comprising extracentrosomal MTs, which extend between the perinuclear compartment and the rostral cytoplasmic swelling (Figures S2C–S2E).

Our ultrastructural observations in combination with immunostaining experiments support the hypothesis that ciliogenesis, CTR subcellular positioning, and centrosomal MT network organization are tightly linked and dynamically regulated during the migration cycle of MGE cells (summarized in Figure 2H). The number of MTs anchored to the centrioles should increase when the mother centriole is docked to the plasma membrane but should decrease as the mother centriole re-positions in the perinuclear cytoplasm. The morphology of the GA is moreover influenced by the MT organization in the centrosomal region since most ninein immunopositive MGE cells presented an elongated GA (Figure S2A). We thus examined whether signals transmitted through the primary cilium could influence the MT organization, the GA conformation, and the migratory behavior of MGE cells.

the centriole pair without interrupting, or end at a distance from centrioles (white arrowheads in C). The plasma membrane is shown in white. The MC docks to the plasma membrane and anchors MTs on lateral appendages (ap). Numerous MTs in the vicinity of the centriole pair do not end on a centriole. Scale bars: (A) and (D), 2 μm. le, leading edge; n, nucleus; sw, swelling.

(G) Histogram shows the preferred orientation of MTs anchored to centrioles located more than 2 μm ahead of the nucleus. Error bars denote SEM.

(H) Interpretative scheme illustrates 4 steps in the migration cycle of MGE cells. During nuclear resting phase (1–3), the centrioles move forward. The MC (yellow) associates with a large distal vesicle occasionally comprising a primary cilium (1, 2). At a distance from the nucleus (n), the MC docks to the plasma membrane and exposes the primary cilium at the cell surface (3). After nuclear translocation along MT bundle comprising extracentrosomal MTs (4), the centrosome removes from the plasma membrane and the primary cilium disappears or internalizes. "+" are MT plus-ends, "−" MT minus-ends. The GA, initially folded around the CTR, unfolds along MTs during forward movement.

See also Figure S2 and Movie S3.

Shh Agonists and Antagonist Influence the Leading Process Morphology in Opposite Ways

MGE cells are generated in the basal forebrain under the control of Shh (Xu et al., 2005) and later migrate in the marginal and intermediate zones of the cortex that expresses Shh at low level (Komada et al., 2008). In vertebrate cells, Shh signal is processed in the primary cilium by a mechanism involving Smoothened (Smo) translocation to the ciliary membrane (Huangfu et al., 2003; Huangfu and Anderson, 2005). We checked that MGE cells migrating either in brain embryo or on dissociated cortical cells or on laminin assemble an adenylate cyclase 3 (AC3) positive primary cilium (Bishop et al., 2007; Sedmak and Wolfrum, 2010; Figure S3). Primary cilium length depended on the substratum of migration (compare Figures S3A and S3F). We first verified that SAG (Smo AGonist) application induced Smo immunoreactivity in the primary cilium of MGE cells (Figure S3E). We then analyzed the response of MGE cells migrating on laminin to Shh and observed unexpected morphological changes in response to the application of agonists (Shh, SAG) and antagonist (cyclopamine) of the Patched1(Ptch)-Smo pathway (Figures 3A–3C2). In cyclopamine treated cultures, MGE cells presented significantly shorter leading processes than in control and in Shh treated cultures (Figure 3C1). MTs could organize in short and thick bundles (Figure 3C2). MTs in the leading process of MGE cells exposed to Shh or SAG often formed a tight bundle in front of the nuclear compartment (opened arrowheads in Figure 3B). MT bundles in Shh treated MGE cells were significantly tighter than in control MGE cells (Figure 3C2; t test, p = 0.033). According to our observations linking the GA morphology to the MT network organization, agonists and antagonist of the Ptch-Smo pathway induced GA conformation changes (Figures 3D–F2). Shh increased the frequency of cells with folded GA whereas cyclopamine increased the frequency of cells with fragmented GA (Figure 3F1). Moreover Shh prevented the GA from entering the leading process and maintained AKAP450, a scaffold protein of the *cis*-Golgi that links the centrosome (Takahashi et al., 1999) in the perinuclear compartment (Figure 3E, bottom raw). Similar GA transformations were observed in MGE cells that migrated on cortical cells (Figure 3F2). Shh signal thus influenced the organization of the MT cytoskeleton and of the endomembrane compartment in MGE cells.

Kif3a Invalidation Impairs MGE Cell Distribution In Vivo

To analyze the consequence of abnormal primary cilium function on the cortical distribution of MGE cells in vivo, we generated mice with $Kif3a^{-/-}$ MGE cells (noted *Kif3a* CKO) by crossing $Kif3a^{fl/fl}$ mutant mice (Marszalek et al., 2000) with *Nkx2.1-Cre, R26R-GFP* transgenic mice whose MGE cells express the GFP (Kessaris et al., 2006). *Kif3a* invalidation impairs anterograde IFT required for cilium assembly and for the processing of Shh signals in the primary cilium (Huangfu et al., 2003; Han et al., 2008; Spassky et al., 2008). The basal telencephalon of *Kif3a* CKO embryos did not show gross morphological abnormalities. At E14.5 and E16.5, Nkx2.1 and Gsx2, two markers of ventral telencephalon patterning (Xu et al., 2005) were expressed in the same areas of both CKO and control embryos, showing that Shh signaling disruption in the MGE at late embryonic stage

had poorly affected the patterning of the ventral telencephalon when MGE cells started migrating (Figure S4). However, at E13.5 and E14.5, the density of GFP(+) $Kif3a^{-/-}$ MGE cells in the cortical tangential migratory streams of CKO embryos was increased two-fold by comparison with the density of GFP(+) $Kif3a^{+/+}$ MGE cells in the cortical tangential migratory streams of control embryos (Figures 4A–4C).

At birth, $Kif3a^{-/-}$ MGE cells had invaded the cortical primordium but their cortical distribution was still abnormal compared to control MGE cells, with increased density of GFP(+) $Kif3a^{-/-}$ MGE cells in the intermediate zone (IZ) and CP (Figures 4D1–4E). Within the CP, cell bodies of $Kif3a^{-/-}$ MGE cells could form radially elongated cluster or chains, which was not observed in control newborn.

In young adults, the number of GFP(+) $Kif3a^{-/-}$ MGE cells was decreased in the granular and supragranular layers of the parietal cortex (Figures 5A and 5B). The dentate gyrus, the most distant cortical structure from the MGE was severely depleted in GFP(+) $Kif3a^{-/-}$ MGE cells (Figures 5C and 5E). Accordingly, somatostatin (SST) positive interneurons were significantly less numerous in this hippocampal area (Figure 5F). The number of SST(+) interneurons was also decreased in the parietal cortex (4 mutant brains, 83% of 4 control brains) and in CA1 and CA3 fields. However, differences missed to reach significance due to irregular distribution of SST(+) interneurons in both control and CKO brains. SST(+) cell bodies in the stratum oriens of CKOs showed abnormal positioning, in agreement with a migration defect (Figure 5D, white arrows).

In *Kif3a* CKOs, the number of parvalbumin (PV) expressing interneurons decreased in both supra- and infragranular layers in all examined neocortical areas (Figures S5A–S5C; mean decrease 68%, p < 0.01) but did not significantly change in the hippocampus. Results in neocortex agree with previous analyses in other models of Shh signaling loss (Xu et al., 2005). In contrast, they differed from counting of GFP(+) MGE cells in *Kif3a* CKOs (Figures 5B, S5D, and S5E). Since most PV(+) interneurons originate in the MGE, this discrepancy could reflect abnormal progenitor differentiation resulting from Shh signal disruption (Figure S4; Xu et al., 2005, 2010).

Both *Kif3a* Invalidation and *Ift88* Invalidation Alter the Migration of MGE Cells to the Cortical Plate

Abnormal distributions of GFP(+) MGE cells in *Kif3a* CKOs at embryonic, neonatal and adult stages were suggestive of abnormal migratory properties of $Kif3a^{-/-}$ MGE cells. To further characterize this defect, we performed time-lapse confocal imaging of cortical slices from E14.5 $Kif3a^{+/+}$, Nkx2.1-Cre, R26R-GFP (control) and E14.5 *Kif3a* CKO embryos. In slices from control embryos, numerous GFP(+) MGE cells located in the deep tangential migratory stream at the start of the recording session, migrated either to the CP or to the ventricular zone (60% of tracked MGE cells; Figures 6A and 6B; see Movie S4). In slices from *Kif3a* CKO embryos, the majority of GFP(+) $Kif3a^{-/-}$ MGE cells located in the deep tangential stream at the start of the recording session stayed migrating within this flow (58% of tracked cells; Figures 6A and 6B; see Movie S4). Although $Kif3a^{-/-}$ MGE cells were able to translocate as fast as control MGE cells in slices (Figure 6C3) and in

Figure 3. Shh Agonists and Antagonist Influence MT Organization and GA Shape in Migrating MGE Cells

(A–C2) Migration on laminin. Panels in (A) compare the distribution of MGE cells around their explant (Exp) of origin after SAG (middle) or cyclopamine (right) treatment. Panels in (B) illustrate the morphology at higher magnification of MGE cells immunostained with anti-tyrosinated tubulin (green) and anti-adenylate cyclase 3 (AC3, red) antibodies. AC3 antibodies label the cytoplasm of MGE cells in addition to the primary cilium (white arrow head). AC3 labeling remains in the perinuclear compartment of SAG treated MGE cells (middle panel, white arrow) but largely distributes in the leading process of cyclopamine treated MGE cells (right panel, white arrow). (C1 and C2) Leading process length and thickness of MGE cells labeled with anti-tyrosinated tubulin antibodies were measured in control (medium gray) and in cyclopamine- (Cycl., black), SAG- (light gray), and Shh- (white) treated cultures. Error bars denote SEM. See text.

(D) In migrating MGE cells, the CTR433 positive median GA either forms a ribbon folded around the CTR (1), or elongates between the nuclear compartment and rostral swelling (2) or splits in fragments (3).

(E–F2) The shape and localization of the median GA (median row in E) is influenced by Shh and cyclopamine treatments. In Shh treated MGE cells, the AKAP450 positive *cis*-GA (bottom row in E) accumulates at one pole of the nucleus, whereas it can enter the leading process of control and cyclopamine treated MGE cells. (F1 and F2) Quantifications of GA shape shows that the GA is more frequently folded in Shh-treated MGE cells and more frequently fragmented in cyclopamine treated MGE cells. Frequencies of the three classes of GA shape in treated cultures were compared to their frequencies in control cultures by a Khi2 test. Statistical differences are indicated by stars above columns. Stars within colored areas indicate statistical differences between control and experimental values in a single class of the distribution (Fisher test, $p < 0.05$). Scale bars: (B), 10 μm; (E), 5 μm.

See also Figure S3.

cocultures (Figures S6A–S6C), their mean migration speed in slices was significantly reduced due to long and frequent stops (Figures 6C1 and 6C2).

We then examined if MGE cells invalidated for *Ift88* (Haycraft et al., 2007) were impaired in their migratory behavior. GFP(+) *Ift88*$^{-/-}$ MGE cells grafted in E14.5 organotypic cortical slices

Figure 4. *Kif3a* Invalidation Impairs MGE Cells Distribution in the Cortical Tangential Migratory Streams and Alters the Cortical Distribution of MGE Cells at Birth

(A–C) $Kif3a^{-/-}$ MGE cells form denser cortical tangential migratory streams. Frontal forebrain sections in (A) compare the cortical distribution of GFP(+) $Kif3a^{+/+}$ MGE cells in E14.5 $Kif3a^{+/+}$; *Nkx2.1-Cre; R26R-GFP* control embryos (top) and the cortical distribution of GFP(+) $Kif3a^{-/-}$ MGE cells in E14.5 $Kif3a^{fl/fl}$; *Nkx2.1-Cre; R26R-GFP* CKO embryos (bottom). Black and white panels are enlarged views of tangential migratory streams in the deep intermediate zone (IZ, arrow heads) and in the superficial marginal zone (MZ, arrows). (B and C) Cell body counted with a confocal microscope in small areas in the deep tangential stream (B, white boxes, 15 μm thick) revealed a two-fold increase in GFP(+) MGE cell density in *Kif3a* CKOs (white bar in histogram C; error bars denote SEM; t test, p < 0.001).

(D1 and D2) Distribution of GFP(+) MGE cells in frontal forebrain sections from control (left) and CKO (right) newborns. Enlarged views (D2) of the median lateral and posterior cortex show that the density of GFP(+) MGE cells is increased in both the MZ and cortical plate (CP) of CKOs. GFP(+) $Kif3a^{-/-}$ MGE cells distribute radially in the CP.

(E) Fluorescence intensity was measured under a large line (yellow) perpendicular to the brain surface to assess the density of GFP(+) MGE cells. Curves were normalized to MZ staining. In CKO brains (yellow curve) that had an enlarged peak of GFP staining in the MZ, the fluorescence intensity in the CP was thus minored (dotted line in graphs indicates the limit between CP and IZ). Scale bars: (A), 500 μm; (B), 100 μm; (D2), 200 μm.

See also Figure S4.

(Figure 6D) showed the same migratory defects as $Kif3a^{-/-}$ MGE cells (Figures 6E–6I). Both mutant cells failed to efficiently colonize the CP (Figures 6E, 6F, 6H, and S6E1–S6F; see Movie S5) and showed more frequent stops (Figure 6G2). The trajectories of both $Ift88^{-/-}$ and $Kif3a^{-/-}$ MGE cells were more erratic than those of control MGE cells (Figures 6F, 6I, S6B, and S6D). $Ift88^{-/-}$ MGE cells exhibited frequent 180° to 360° turns and occasional polarity reversals (Figure 6J). Both $Ift88^{-/-}$ and $Kif3a^{-/-}$ MGE cells were thus less efficient than control MGE cells to sustain directed migration and failed to colonize the cortical plate.

$Kif3a^{-/-}$ and $Ift88^{-/-}$ MGE Cells Show Abnormal Orientation in the Deep Tangential Migratory Stream

MGE cells migrate to the CP along radial glial cells (Yokota et al., 2007), blood vessels (Le Magueresse et al., 2012) and possibly along corticofugal axons, as suggested by their oblique trajectories (Tanaka et al., 2003) and by contacts with growth cones in the cortical SVZ (Métin et al., 2000). Several studies have shown that MGE cells migrating tangentially in the developing cortex reorient from the deep and superficial tangential migratory streams to the CP by neoforming side branches in front of the nucleus (Martini et al., 2009; Lysko et al., 2011). We examined the
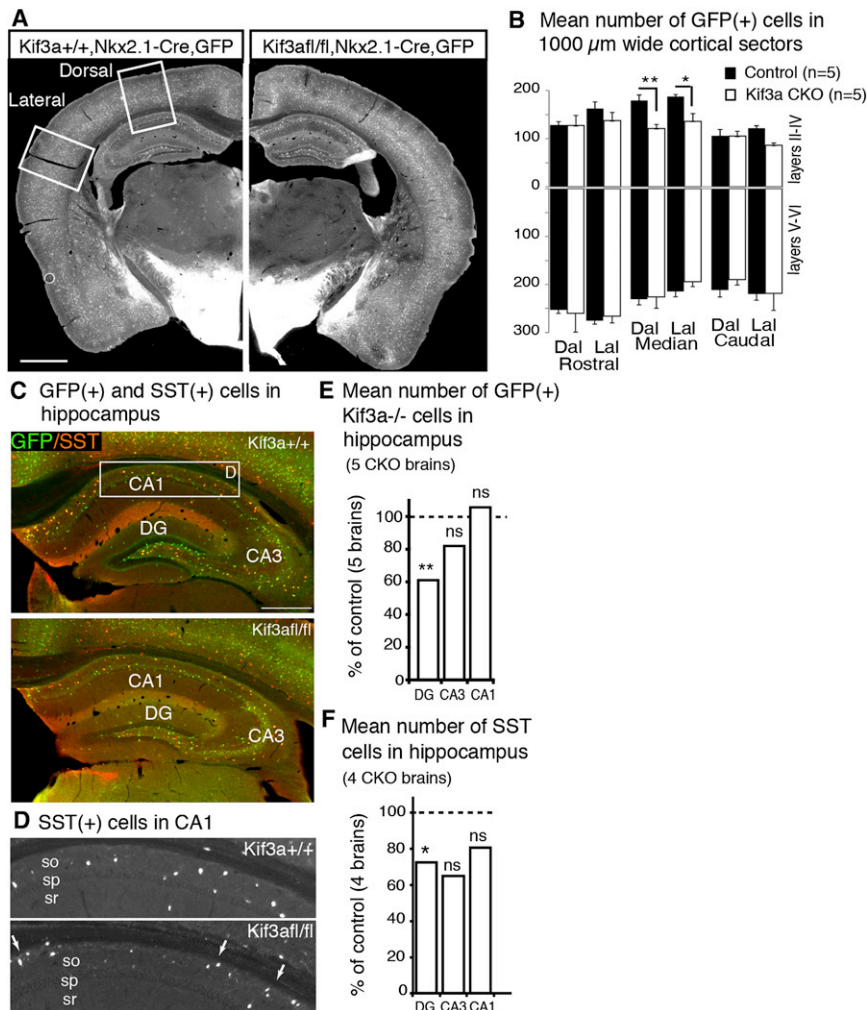
Figure 5. *Kif3a* Invalidation Alters the Cortical Distribution of MGE Cells at Adult Stage

(A and B) GFP(+) MGE cells were counted in precisely located dorsal and lateral 1,000 μm wide cortical sectors, on frontal sections at 3 rostrocaudal levels (see details in Figure S5). Brain hemisections in (A) are from control (left) and *Kif3a* CKO (right) young adults (P30–45). GFP(+) *Kif3a*$^{-/-}$ MGE cells were significantly less numerous in the supragranular layers of the adult parietal cortex than *Kif3a*$^{+/+}$ GFP(+) MGE cells (B, median level). Histogram shows mean values; error bars denote SEM.

(C–F) In adult CKOs, the number of GFP(+) *Kif3a*$^{-/-}$ MGE cells was strongly reduced in the dentate gyrus (DG: C and E). In hippocampus, most somatostatin (SST) expressing cells (C, red cells) were GFP positive. The number of SST(+) cells was significantly decreased in the DG of CKOs (F). Panels in (D) illustrate the change in SST(+) cells positioning in the stratum oriens (so) of control (top panel) and CKO (bottom panel, white arrows) brains. Sp, stratum pyramidale; sr, stratum radiatum. In (E) and (F), mean values are shown as percentage of the mean control value. Statistical differences in (B), (E), and (F) were tested with the Mann-Whitney U test. Scale bars: (A), 1,000 μm; (C), 500 μm.

See also Figure S5.

morphology of *kif3a* or *Ift88* invalidated MGE cells in grafted cortical slices where MGE cell density allowed detailed morphological analyses on large samples. The leading process of both *Kif3a*$^{-/-}$ and *Ift88*$^{-/-}$ MGE cells was significantly more branched than in control MGE cells (Figures 7A–7C) but showed minimal changes in length (Figure 7D). Migrating MGE cells continuously produce branches at cell front and retract branches not selected for nuclear progression (Bellion et al., 2005, Métin et al., 2006; Martini et al., 2009). *Kif3a*$^{-/-}$ and *Ift88*$^{-/-}$ MGE cells produced branches at the same rate as control MGE cells, except a fraction of *Ift88*$^{-/-}$ MGE cells arrested under the CP, which actively extended processes. Both eliminated slowly nonselected branches. In *Kif3a*$^{-/-}$ MGE cells migrating on a homogeneous substratum of cortical cells, the time life of transient branches was increased by 60% (Figure 7E). Alteration in leading process remodeling was associated to minor defects in centrosome positioning (Figures S7A–S7C) and did not favor directional changes. In organotypic slices, grafted *Kif3a*$^{-/-}$ and *Ift88*$^{-/-}$ MGE cells located in the deep tangential stream oriented parallel to each other, tangential to the CP whereas grafted wild-type MGE cells exhibited wider range of orientations compatible

with re-orientation toward the CP (Figures 7F1 and 7F2). In *Kif3a* CKO embryos, the leading processes of *Kif3a*$^{-/-}$ MGE cells oriented parallel to each other, and sometimes fasciculated on each other (white arrow heads in Figure 7G). Similarly, cultured *Kif3a*$^{-/-}$ MGE cells aggregated in small clusters or fasciculated on each other in vitro (Figures S7D–S7E2). They failed to reorient on a parallel array of cortical axons, in contrast to wild-type MGE cells (Figures S7F1–S7G).

Altogether, these results show that abnormal IFT alters the capacity of MGE cells to select a novel direction of migration by impairing dynamic reorganizations of the leading process but minimally interferes with nuclear motility (Figures 6C3 and S6C). Abnormal leading process dynamics is moreover associated to abnormal interactions between MGE cells.

Shh Signaling Influences MGE Cell Migration to the Cortical Plate

Functional IFT is required for the normal processing of Shh signals in the primary cilium (Huangfu et al., 2003; Louvi and Grove, 2011). To confirm that the abnormal migratory behavior of MGE cells invalidated for *Kif3a* or *Ift88* resulted from abnormal processing of Shh signals in the Ptch-Smo pathway, we examined the influence of agonists and antagonist on the distribution of wild-type MGE cells grafted in cortical slices (Figures 8A1–8C). In cyclopamine treated slices, wild-type MGE cells distributed in a narrow and deep stream tangential to the CP and
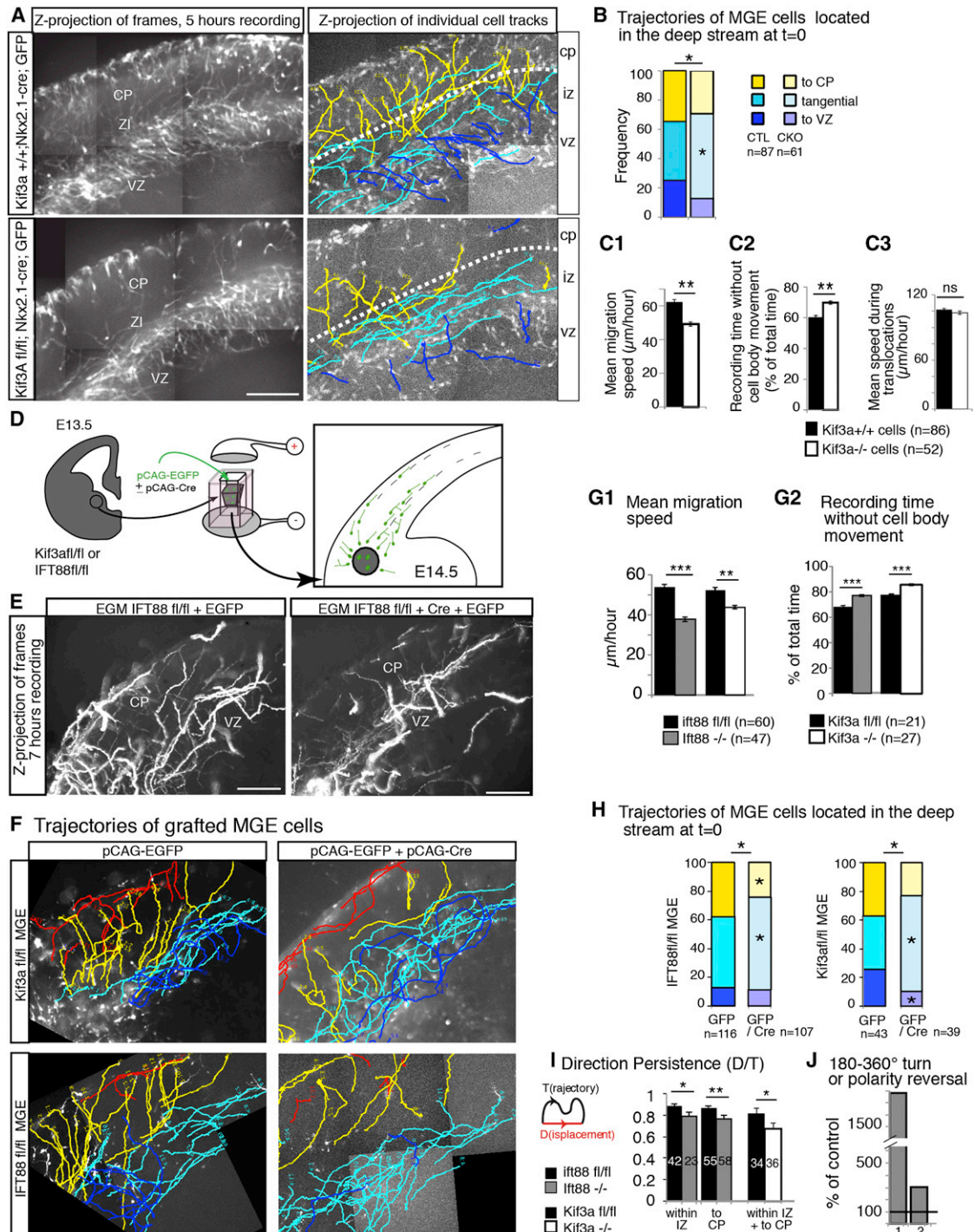
Figure 6. *Kif3a*^{−/−} and *Ift88*^{−/−} MGE Cells Fail to Enter the Cortical Plate

(A) Cortical slices from E14.5 control (upper row) and *Kif3a* CKO (bottom row) embryos were imaged with a confocal microscope each 3 min. Confocal frames acquired each 3 μm to a thickness of 30 microns were projected on a single plane to generate movies. Left panels are Z-projections of pictures from movies. Numerous GFP(+) *Kif3a*^{+/+} (top) and *Kif3a*^{−/−} (bottom) MGE cells migrate within the intermediate zone (IZ). Right panels show the trajectories of individual GFP(+) MGE cells imaged in this deep flow during at least five consecutive frames. Trajectories were oriented to the cortical plate (CP, yellow), to the ventricular zone (VZ, dark blue), or maintained within the intermediate zone/subventricular zone (IZ/SVZ, light blue).

(B) *Kif3a*^{−/−} MGE cells migrated more frequently within the IZ/SVZ than *Kif3a*^{+/+} MGE cells.

(C1–C3) Compared to *Kif3a*^{+/+} MGE cells (black bars), *Kif3a*^{−/−} MGE cells (white bars) showed reduced mean migration speed (C1) because of longer and more frequent resting phases (C2). The dynamics of cell body movements was unchanged (C3).

(legend continued on next page)

oriented parallel to each other (Figures 8A2, 8A3, and 8B), mimicking the behavior of *Kif3a* or *Ift88* invalidated MGE cells (Figure 7). In Shh and SAG treated slices in contrast, MGE cells largely scattered and reoriented radially toward the CP (Figures 8A2, 8A3, and 8B). Shh signals thus favored MGE cell exit from the deep tangential migratory stream. MGE cell response to Shh was IFT dependent since neither cyclopamine nor Shh application modulated the density of *Kif3a*$^{-/-}$ MGE cells in the CP of organotypic slices from *Kif3a* CKOs embryos (Figure 8F).

Both cyclopamine and Shh increased the proportion of MGE cells with branched leading processes in grafted slices (Figure 8C). The Shh phenotype involves a Ptch-Smo dependent signaling mechanism since it was reversed by *Ift88* invalidation (Figure 8C, compare black, green and light green bars).

Perturbations of the Shh signaling pathway altered the directionality of MGE cells, the time life of their processes, but not their migration speed (Figures 8D1–8D3, S8A, and S8B and Movies S7 and S8). Careful examination of movies showed that Shh stabilized the trailing processes and associated to numerous polarity reversals whereas cyclopamine increased the time life of the leading process. Accordingly, cyclopamine increased the time life of the rostral swelling that comprises the CTR/GA complex whereas Shh did the opposite (Figures S8C–S8F). These results agree with morphological changes of MGE cells described above (Figure 3E).

Using immunostaining, Komada et al. (2008) had previously shown that Shh is present in the developing cortex. Here, we confirmed using in situ hybridization that *Shh* is already expressed in the IZ of the cortical wall at E14.5 (Figure 8E1), the stage when MGE cells start to colonize the cortical plate. The expression pattern of *Shh* is compatible with local and discrete modulation of leading processes properties all along the migratory pathway of MGE cells (Figure 8E2).

DISCUSSION

Our study shows that the mother centriole of tangentially migrating GABA neurons assembles a primary cilium and docks to the plasma membrane through this primary cilium. The primary cilium of tangentially migrating GABA neurons is functional and transduces local Shh signal that promotes GABA neurons reorientation from tangential migratory streams toward the cortical plate (CP). Using complementary genetic models, we show that functional anterograde IFT is required for Shh dependent reorientation of interneurons toward the CP during embryonic development and influences cortex colonization by GABA neurons.

It is established that the CTR controls the neuronal migration through its MTOC function (Higginbotham and Gleeson, 2007). In tangentially migrating MGE cells, the CTR anchors a MT network distinct from extracentrosomal MTs. The centrosomal array of MTs is reminiscent of the cage of perinuclear MTs described in radially migrating neurons (Rivas and Hatten, 1995; Solecki et al., 2004; Tsai et al., 2007). Bundles of extracentrosomal MTs extend in front of the nucleus, as already described in cerebellar neurons (Umeshima et al., 2007). This MT organization into two networks should support quick changes in the relative positioning of the CTR and nucleus and should permit independent movements of the CTR toward the plasma membrane, allowing fusion between the centriolar vesicle and the plasma membrane. Plasma membrane docking of the mother centriole should position the centrosomal network of MTs on one side of the leading process, thereby influencing cell directionality. Strong correlation between the subcellular location of the mother centriole and its distance to the nucleus suggests that the mother centriole is not permanently docked to the plasma membrane during the migratory cycle. Rather, the primary cilium is successively addressed and removed from the cell surface by fusion/fission of the centriolar vesicle. An important question for the future will be to understand how the subcellular localization of the mother centriole during the migration cycle is correlated to ciliogenesis and to trajectory decisions.

The primary cilium of MGE cells varied in length depending on the substratum of migration. Differences could result from difference in adhesive interactions between MGE cells and their migratory substratum since it has been shown that contact interactions and the distribution of tension forces affect primary cilium length in adhesive mammalian cells (Pitaval et al., 2010). Differences could also result from change in microtubule stability and in signaling pathway activity (Massinen et al., 2011). Indeed, we have observed that MGE cells cultured in the presence of agonists of the Patched1-Smoothened (Ptch-Smo) pathway have longer primary cilia.

Another major finding of our study is that the primary cilium of migrating MGE cells transduces Shh signal through a mechanism involving the Ptch-Smo signaling pathway. Shh is expressed in the migratory pathway of MGE cells (Komada et al., 2008 and this study). Smo immunostaining was observed in the primary cilium of MGE cells cultured in the presence of Shh or SAG, confirming a central role of the primary cilium in Shh signaling. *Kif3a*$^{-/-}$ MGE cells, *Ift88*$^{-/-}$, MGE cells, and cyclopamine treated MGE cells showed similar migratory defects that very likely resulted from impaired transduction of Shh signal in

---

(D–J) Migration of *Ift88*$^{-/-}$ and *Kif3a*$^{-/-}$ MGE cells grafted in organotypic cortical slices. (D) Small MGE explants from *Ift88*$^{fl/fl}$ or *Kif3a*$^{fl/fl}$ embryos were coelectroporated with *pCAG-EGFP* and *pCAG-Cre* and grafted at the pallium/subpallium boundary in E14.5 wild-type forebrain slices (right panels in E and F). Control explants were electroporated with *pCAG-EGFP* only (left panels in E and F). GFP(+) MGE cells were imaged in slices with either a fluorescent macroscope (E) or a confocal microscope (F). Panels in (E) are Z projections of movies. Panels in (F) are pictures obtained as explained in (A) (same color code for trajectories, red trajectories started in marginal zone). (G1 and G2) Both *Ift88*$^{-/-}$ (gray bars) and *Kif3a*$^{-/-}$ (white bars) MGE cells showed slower migration speed (G1) and longer resting phases (G2) than control MGE cells (black bars). (H) Both *Ift88*$^{-/-}$ and *Kif3a*$^{-/-}$ MGE cells preferentially migrated within the deep tangential migratory stream instead of reorienting toward the CP or VZ. I. In both IZ and CP, the direction persistence (distance of displacement /trajectory length) of *Ift88*$^{-/-}$ and *Kif3a*$^{-/-}$ cells was significantly reduced by comparison to control cells. (J) *Ift88*$^{-/-}$ MGE cells show frequent 180° to 360° turns. Scale bars, 200 μm. Statistical differences between distributions (B and H) assessed as explained in Figures 3F1 and 3F2. Histograms show mean values, error bars denote SEM, and stars indicate statistical differences (t test).
See also Figure S6, Movie S4, and Movie S5.
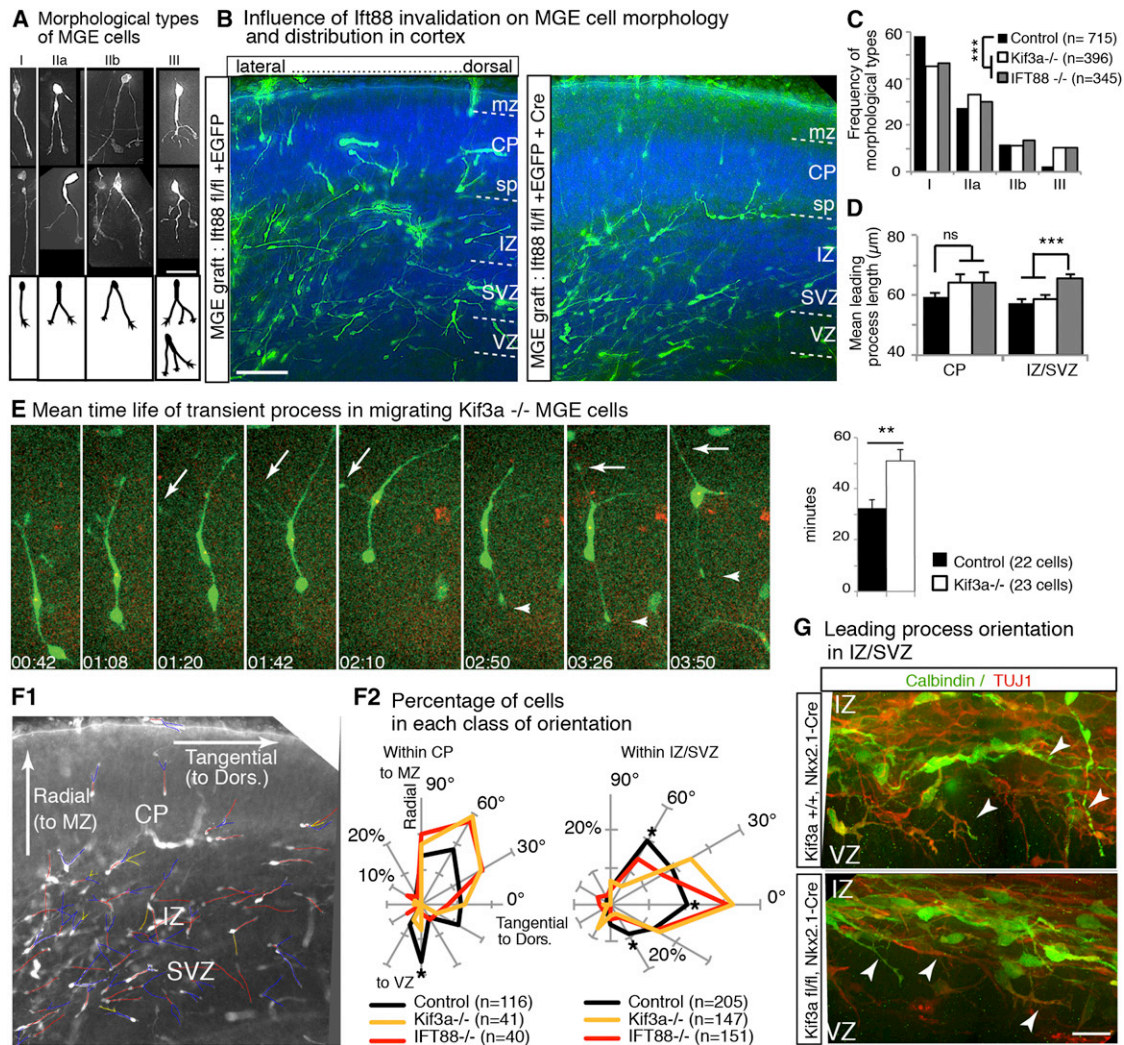
Figure 7. *Kif3a* or *Ift88* Invalidated MGE Cells Grafted in Cortical Slices Show Alteration in Leading Process Morphology and Orientation

(A) Confocal pictures and drawing illustrate our simplified classification of MGE cells.

(B) Panels illustrate the distribution, orientation, and morphology of GFP(+) *Ift88*$^{fl/fl}$ MGE cells (electroporated with *pCAG-EGFP*, left panel) and of GFP(+) *Ift88*$^{-/-}$ MGE cells (coelectroporated with *pCAG-EGFP* and *pCAG-Cre*, right panel) grafted in cortical slices. Nuclear staining (bisbenzimide, blue) reveals cortical wall cytoarchitecture.

(C and D) Analyses in cortical slices show that *Kif3a* and *Ift88* invalidation significantly increased the frequency of MGE cells with branched leading process.

(E) Branch dynamics in *Kif3a*$^{-/-}$ MGE cell. Time-lapse sequence illustrates the migration on E14.5 dissociated cortical cells of a *Kif3a*$^{fl/fl}$ MGE cell co-electroporated with *pCAG-EGFP* and *pCAG-Cre*. Time is in hour/minute on frames. White arrows indicate transient branches, white arrowhead the trailing process. Histogram on the right shows the mean increase in time life of leading and trailing processes in *Kif3a*$^{-/-}$ MGE cells. Errors bars in histograms (D) and (E) denote SEM.

(F1 and F2) Leading process orientation of *Ift88*$^{-/-}$ and *Kif3a*$^{-/-}$ MGE cells migrating in cortical slices. (F1) NeuronJ software was used to calculate the angular deviation of each leading process with regard to the cortical plate (CP) surface. Processes oriented radially to the marginal zone (MZ) have an angular deviation of +90°. (F2) Polar plots show the frequency of leading process orientations. In the intermediate zone/subventricular zone (IZ/SVZ), the majority of mutant cells oriented preferentially in the [−30°,+30°] range, whereas control MGE cells presented a wider range of orientations [−60°,+60°]. Distributions of preferred orientations significantly differed in the −60°/90° range between control and mutant MGE cells (Khi2 test, p < 0.001). Stars indicate significant differences between individual values in orientation distributions (Fisher test; p < 0.05).

(G) In the lower IZ of E14.5 control (top panel) and CKO (bottom panel) embryos immunostained with anti-calbindin (green) and anti-βIII-tubulin (red) antibodies, calbindin positive cells of the CKO are closely parallel to each other. sp, subplate, vz, ventricular zone. Scale bars: (A), 20 μm; (B), 100 μm; (G), 50 μm.

See also Figure S7 and Movie S6.

the primary cilium of migrating MGE cells. Although Shh functions as a chemo-attractant for tangentially migrating SVZ cells (Angot et al., 2008) and as a chemoattractant or -repellent for

growing axons (Charron et al., 2003; Sánchez-Camacho and Bovolenta, 2009), neither clear attractive nor clear repulsive activity of Shh on MGE cells was observed in organotypic slices. Rather,
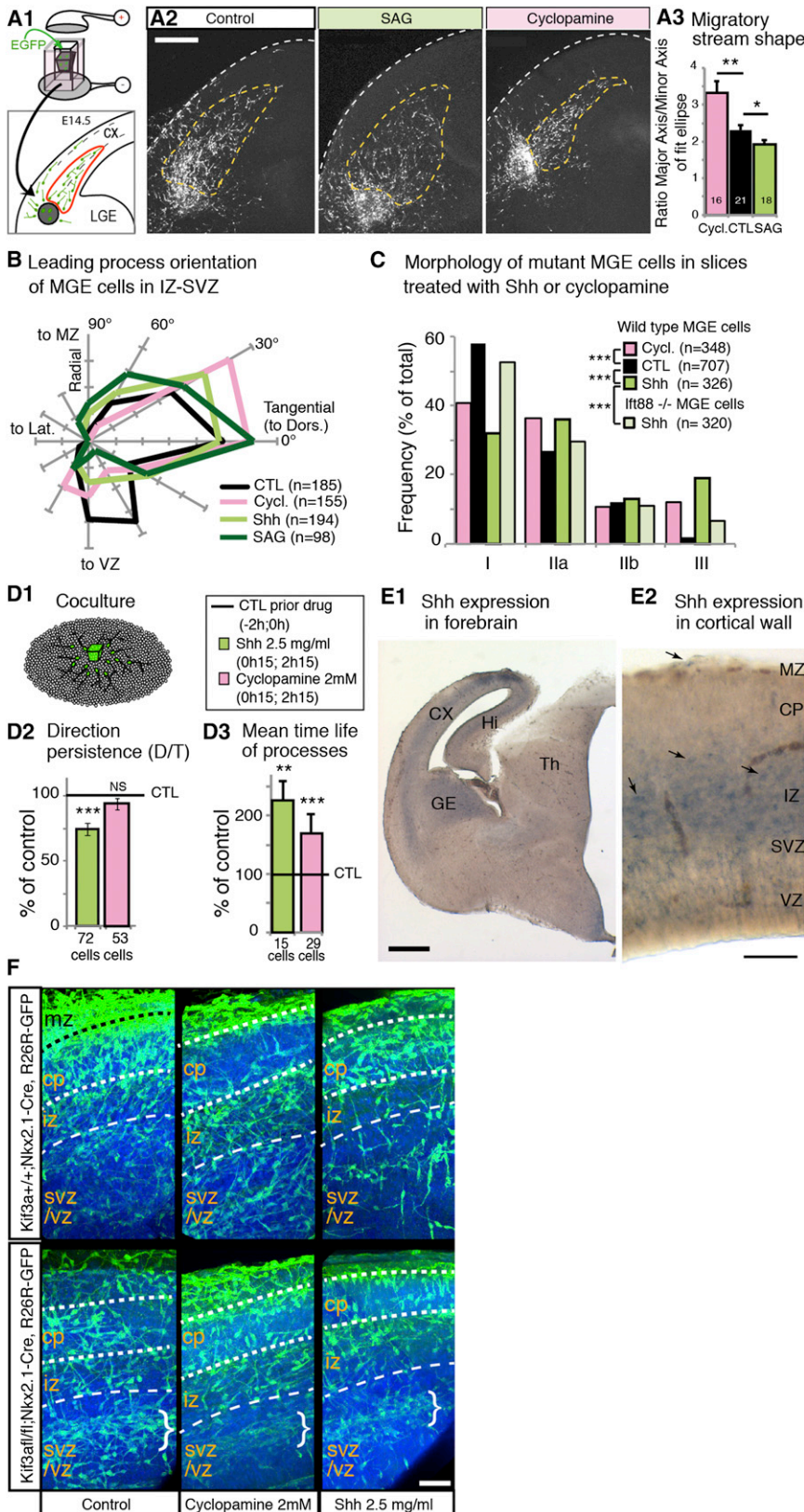
Figure 8. Influence of Shh and Cyclopamine on MGE Cell Migration in Brain Slices and In Vitro

(A1–B) Wild-type MGE cells electroporated with *pCAG-EGFP* and grafted at the pallium/sub-pallium boundary in organotypic forebrain slices (A1) distribute in a large and deep tangential migratory stream after 24 hr in culture (A2, control frame). In cyclopamine-treated slice, grafted MGE cells form a tight stream (right frame in A2, pink bar in A3; significantly narrower fit ellipse, p = 0.0024) while they scatter in Shh treated slices (middle frame in A2, green bar in A3, significantly larger fit ellipse, p = 0.044). Analysis of leading process orientation (as explained in Figure 7F1) reveals that MGE cells orient preferentially tangential to the cortical plate (CP) in cyclopamine treated slices (B, pink curve significantly different from black control curve by Khi2 test, p = 0.001) and more often radially in Shh and SAG treated slices (B, green curves significantly different from black control curve by Khi2 test, p = 0.013 for Shh, p < 0.001 for SAG).

(C) Morphological analyses similar to those illustrated in Figures 7A and 7C show that both cyclopamine and Shh treatment significantly increase the proportion of MGE cells with a branched leading process (percentages of cells in classes IIa and III significantly increased at the expense of class I, Khi2 test, p < 0.001).

(D1–D3) Shh application on MGE cells migrating on dissociated cortical cells (D1) induces frequent changes of MGE cell direction. The direction persistence is significantly decreased (D2, green bar). Both Shh and cyclopamine strongly increase the time life of MGE cell processes (D3).

(E1 and E2) In situ hybridization of forebrain section with an antisens probe shows low *Shh* expression in the intermediate zone (IZ) of the cortical wall at E14.5 (E1). At higher magnification (E2), the DIG reaction product (blue) labels cell bodies (black arrows) in the IZ and upper sub-ventricular zone (SVZ), a few cells at the top of the marginal zone (MZ, black arrow) and radially oriented cell bodies and processes in the ventricular zone (VZ).

(F) Pictures are Z-projection of 20 confocal planes acquired each 1 μm in the cortical wall of forebrain slices from E14.5 control (upper row) and *Kif3a* CKO (lower row) embryos. Slices were collected at the same rostrocaudal level and cultured in control condition (left) or in the presence of either cyclopamine (middle) or Shh (right). Cyclopamine prevented GFP(+) *Kif3a*^{+/+} MGE cells from entering the CP (upper middle panel), whereas Shh promoted CP colonization by MGE cells (upper right panel). GFP(+) *Kif3a*^{−/−} MGE cells (lower panels) did not change their CP distribution in response to cyclopamine or Shh and formed a dense tangential migratory stream (accolade). Stars in (C) show the significance level of Khi2 test; stars in (A3), (D2), and (D3) show the significance level of t test (error bars in histograms denote SEM). Scale bars: (A2), 200 μm; (E1), 500 μm; (E2 and F), 100 μm.

See also Figure S8, Movie S7, and Movie S8.

the primary cilium controlled the migration of MGE cells in a context dependent manner and facilitated MGE cell reorientation. Functional IFT prevented MGE cells to fasciculate on each other suggesting that signals transmitted through the primary cilium mediate repulsive interactions between migrating MGE cells and/or promotes adhesive interactions with other cells. It is established that future interneurons are maintained by CXCL12/CXCR4 mediated attractive interactions in their tangential cortical routes (Stumm et al., 2003; López-Bendito et al., 2008; Lysko et al., 2011). From early developmental stages, however, some neurons leave the tangential migratory streams to enter the CP (Tanaka et al., 2003). Shh signal in the developing cortex promotes this process. Although interactions between migrating MGE cells and cortical axons are poorly documented in vivo (Métin et al., 2000; Pinheiro et al., 2011), our results suggest that Shh signal could orient the migration of MGE cells toward the cortex along corticofugal axons or radial glia. Abnormal orientation of migrating MGE cells along these guiding structures might be responsible for the decreased number of $Kif3a^{-/-}$ cells that we observed in the supragranular layers of the parietal cortex.

In conclusion, our study establishes that the CTR of long distance tangentially migrating GABA neurons regulates the migration of these neurons by gathering in a same area the GA through its *cis*-compartment, centrosomal MTs, and signaling pathways associated to the primary cilium. Shh signals transduced by the primary cilium prevented the aggregation of MGE cells in the cortical tangential migratory streams and helped MGE cells to leave tangential streams and to re-orient toward the CP, thereby acting to maintain an optimal density of MGE cells in the cortical primordium. We thus identified the primary cilium and the associated CTR as a signaling center able to convert extrinsic signals into morphological changes to influence cell movements. The mechanism(s) by which Shh signal influenced the organization of the MT cytoskeleton and the subcellular distribution of the endomembrane system in the leading process of MGE cells, is unknown. This cellular response to Shh signal has never been described previously. It nevertheless provides a cellular basis for better understanding the defects in long distance neuronal migration associated with mutations in centriolar (Endoh-Yamagami et al., 2010) or basal body proteins, the so-called BBS proteins (Tobin et al., 2008). It should help to further analyze abnormal cognitive functions associated to defects in primary cilium structure or function.

EXPERIMENTAL PROCEDURES

Detailed description of methods in Supplemental Experimental Procedures.

Mice

Mice from the following strains were used at embryonic or adult stage: Swiss (Janvier, France), $Kif3a^{fl/fl}$, $Ift88^{fl/fl}$, and $Nkx2.1$-Cre; Rosa26R-GFP (or YFP). Our experimental procedures were reviewed and approved by the Regional Ethic Committee for Animal Experiment.

Electron Microscopy

Cultures prepared on plastic coverslips were fixed, embedded in araldite, contrasted and sectioned in semithin sections. Sections were used to acquire tomography series with an energy-filtered transmission high-voltage electron microscope. Tomogram reconstruction and 3D models were performed with Etomo and IMOD softwares (Boulder University).

Cultures and Videomicroscopy

MGE explants electroporated with expression vectors (*pCAG-EGFP, pCAG-Cre, pCAG-PACT-mKO1*) were cultured on laminin, on dissociated cortical cells, or on cortical axons. They were imaged with an inverted epifluorescence microscope or with an inverted microscope equipped with a spinning disk, using either a ×40 or a ×63 immersion objective. Organotypic slices from transgenic mice, and organotypic slices from wild-type mice grafted with MGE explants were cultured in Millicell chambers (Merck Millipore) and imaged with an epifluorescence macroscope (Olympus) or with an inverted microscope equipped with a spinning disk and a ×20 long distance objective.

Pharmacological treatments were applied in the culture medium: Shh (N-Ter, R&D Systems, 2.5 μg/ml), SAG (Smo agonist, Calbiochem, 10 μM), or cyclopamine (Sigma-Aldrich, 2μM).

Immunohistochemistry and In Situ Hybridization

Floating sections from embryonic or adult brains were immunostained with antibodies against GFP, parvalbumin, somatostatin, Nkx2.1, Gsx2, or AC3. Cultures were immunostained with antibodies against tubulin, γtubulin, *cis*-GA (GMAP210, AKAP450), or median GA (CTR433). MT plus- and minus-ends were revealed with EB1 and ninein antibodies.

Shh ISH was performed on floating sections from embryonic brains.

Softwares for data acquisition and analyses, see Supplemental Experimental Procedures.

SUPPLEMENTAL INFORMATION

Supplemental Information includes eight figures, eight movies, and Supplemental Experimental Procedures and can be found with this article online at http://dx.doi.org/10.1016/j.neuron.2012.10.027.

REFERENCES

Angot, E., Loulier, K., Nguyen-Ba-Charvet, K.T., Gadeau, A.P., Ruat, M., and Traiffort, E. (2008). Chemoattractive activity of sonic hedgehog in the adult subventricular zone modulates the number of neural precursors reaching the olfactory bulb. Stem Cells *26*, 2311–2320.

Arellano, J.I., Guadiana, S.M., Breunig, J.J., Rakic, P., and Sarkisian, M.R. (2012). Development and distribution of neuronal cilia in mouse neocortex. J. Comp. Neurol. *520*, 848–873.

Baird, D.H., Myers, K.A., Mogensen, M., Moss, D., and Baas, P.W. (2004). Distribution of the microtubule-related protein ninein in developing neurons. Neuropharmacology *47*, 677–683.

Baudoin, J.P., Alvarez, C., Gaspar, P., and Métin, C. (2008). Nocodazole induced changes in microtubule dynamics impair the morphology and directionality of migrating MGE cells. Dev. Neurosci. *30*, 132–143.

Bellion, A., Baudoin, J.P., Alvarez, C., Bornens, M., and Métin, C. (2005). Nucleokinesis in tangentially migrating neurons comprises two alternating phases: forward migration of the Golgi/centrosome associated with centrosome splitting and myosin contraction at the rear. J. Neurosci. *25*, 5691–5699.

Besse, L., Neti, M., Anselme, I., Gerhardt, C., Rüther, U., Laclef, C., and Schneider-Maunoury, S. (2011). Primary cilia control telencephalic patterning and morphogenesis via Gli3 proteolytic processing. Development *138*, 2079–2088.

Bishop, G.A., Berbari, N.F., Lewis, J., and Mykytyn, K. (2007). Type III adenylyl cyclase localizes to primary cilia throughout the adult mouse brain. J. Comp. Neurol. *505*, 562–571.

Bornens, M. (2012). The centrosome in cells and organisms. Science *335*, 422–426.

Breunig, J.J., Sarkisian, M.R., Arellano, J.I., Morozov, Y.M., Ayoub, A.E., Sojitra, S., Wang, B., Flavell, R.A., Rakic, P., and Town, T. (2008). Primary cilia regulate hippocampal neurogenesis by mediating sonic hedgehog signaling. Proc. Natl. Acad. Sci. USA *105*, 13127–13132.

Charron, F., Stein, E., Jeong, J., McMahon, A.P., and Tessier-Lavigne, M. (2003). The morphogen sonic hedgehog is an axonal chemoattractant that collaborates with netrin-1 in midline axon guidance. Cell *113*, 11–23.

Christensen, S.T., Pedersen, S.F., Satir, P., Veland, I.R., and Schneider, L. (2008). The primary cilium coordinates signaling pathways in cell cycle control and migration during development and tissue repair. Curr. Top. Dev. Biol. *85*, 261–301.

Cohen, E., Binet, S., and Meininger, V. (1988). Ciliogenesis and centriole formation in the mouse embryonic nervous system. An ultrastructural analysis. Biol. Cell *62*, 165–169.

Distel, M., Hocking, J.C., Volkmann, K., and Köster, R.W. (2010). The centrosome neither persistently leads migration nor determines the site of axonogenesis in migrating neurons in vivo. J. Cell Biol. *191*, 875–890.

Endoh-Yamagami, S., Karkar, K.M., May, S.R., Cobos, I., Thwin, M.T., Long, J.E., Ashique, A.M., Zarbalis, K., Rubenstein, J.L., and Peterson, A.S. (2010). A mutation in the pericentrin gene causes abnormal interneuron migration to the olfactory bulb in mice. Dev. Biol. *340*, 41–53.

Follit, J.A., San Agustin, J.T., Xu, F., Jonassen, J.A., Samtani, R., Lo, C.W., and Pazour, G.J. (2008). The Golgin GMAP210/TRIP11 anchors IFT20 to the Golgi complex. PLoS Genet. *4*, e1000315.

Fuchs, J.L., and Schwark, H.D. (2004). Neuronal primary cilia: a review. Cell Biol. Int. *28*, 111–118.

Gorivodsky, M., Mukhopadhyay, M., Wilsch-Braeuninger, M., Phillips, M., Teufel, A., Kim, C., Malik, N., Huttner, W., and Westphal, H. (2009). Intraflagellar transport protein 172 is essential for primary cilia formation and plays a vital role in patterning the mammalian brain. Dev. Biol. *325*, 24–32.

Han, Y.G., Spassky, N., Romaguera-Ros, M., Garcia-Verdugo, J.M., Aguilar, A., Schneider-Maunoury, S., and Alvarez-Buylla, A. (2008). Hedgehog signaling and primary cilia are required for the formation of adult neural stem cells. Nat. Neurosci. *11*, 277–284.

Haycraft, C.J., Zhang, Q., Song, B., Jackson, W.S., Detloff, P.J., Serra, R., and Yoder, B.K. (2007). Intraflagellar transport is essential for endochondral bone formation. Development *134*, 307–316.

Higginbotham, H.R., and Gleeson, J.G. (2007). The centrosome in neuronal development. Trends Neurosci. *30*, 276–283.

Huangfu, D., and Anderson, K.V. (2005). Cilia and Hedgehog responsiveness in the mouse. Proc. Natl. Acad. Sci. USA *102*, 11325–11330.

Huangfu, D., Liu, A., Rakeman, A.S., Murcia, N.S., Niswander, L., and Anderson, K.V. (2003). Hedgehog signalling in the mouse requires intraflagellar transport proteins. Nature *426*, 83–87.

Kessaris, N., Fogarty, M., Iannarelli, P., Grist, M., Wegner, M., and Richardson, W.D. (2006). Competing waves of oligodendrocytes in the forebrain and postnatal elimination of an embryonic lineage. Nat. Neurosci. *9*, 173–179.

Komada, M., Saitsu, H., Kinboshi, M., Miura, T., Shiota, K., and Ishibashi, M. (2008). Hedgehog signaling is involved in development of the neocortex. Development *135*, 2717–2727.

Konno, D., Shioi, G., Shitamukai, A., Mori, A., Kiyonari, H., Miyata, T., and Matsuzaki, F. (2008). Neuroepithelial progenitors undergo LGN-dependent planar divisions to maintain self-renewability during mammalian neurogenesis. Nat. Cell Biol. *10*, 93–101.

Koster, A.J., Grimm, R., Typke, D., Hegerl, R., Stoschek, A., Walz, J., and Baumeister, W. (1997). Perspectives of molecular and cellular electron tomography. J. Struct. Biol. *120*, 276–308.

Le Magueresse, C., Alfonso, J., Bark, C., Eliava, M., Khrulev, S., and Monyer, H. (2012). Subventricular zone-derived neuroblasts use vasculature as a scaffold to migrate radially to the cortex in neonatal mice. Cereb. Cortex *22*, 2285–2296.

Lee, J.H., and Gleeson, J.G. (2010). The role of primary cilia in neuronal function. Neurobiol. Dis. *38*, 167–172.

López-Bendito, G., Sánchez-Alcañiz, J.A., Pla, R., Borrell, V., Picó, E., Valdeolmillos, M., and Marín, O. (2008). Chemokine signaling controls intracortical migration and final distribution of GABAergic interneurons. J. Neurosci. *28*, 1613–1624.

Louvi, A., and Grove, E.A. (2011). Cilia in the CNS: the quiet organelle claims center stage. Neuron *69*, 1046–1060.

Lysko, D.E., Putt, M., and Golden, J.A. (2011). SDF1 regulates leading process branching and speed of migrating interneurons. J. Neurosci. *31*, 1739–1745.

Marszalek, J.R., Liu, X., Roberts, E.A., Chui, D., Marth, J.D., Williams, D.S., and Goldstein, L.S. (2000). Genetic evidence for selective transport of opsin and arrestin by kinesin-II in mammalian photoreceptors. Cell *102*, 175–187.

Martini, F.J., Valiente, M., López Bendito, G., Szabó, G., Moya, F., Valdeolmillos, M., and Marín, O. (2009). Biased selection of leading process branches mediates chemotaxis during tangential neuronal migration. Development *136*, 41–50.

Massinen, S., Hokkanen, M.E., Matsson, H., Tammimies, K., Tapia-Páez, I., Dahlström-Heuser, V., Kuja-Panula, J., Burghoorn, J., Jeppsson, K.E., Swoboda, P., et al. (2011). Increased expression of the dyslexia candidate gene DCDC2 affects length and signaling of primary cilia in neurons. PLoS ONE *6*, e20580.

Métin, C., Denizot, J.P., and Ropert, N. (2000). Intermediate zone cells express calcium-permeable AMPA receptors and establish close contact with growing axons. J. Neurosci. *20*, 696–708.

Métin, C., Baudoin, J.P., Rakić, S., and Parnavelas, J.G. (2006). Cell and molecular mechanisms involved in the migration of cortical interneurons. Eur. J. Neurosci. *23*, 894–900.

Métin, C., Vallee, R.B., Rakic, P., and Bhide, P.G. (2008). Modes and mishaps of neuronal migration in the mammalian brain. J. Neurosci. *28*, 11746–11752.

Pinheiro, E.M., Xie, Z., Norovich, A.L., Vidaki, M., Tsai, L.H., and Gertler, F.B. (2011). Lpd depletion reveals that SRF specifies radial versus tangential migration of pyramidal neurons. Nat. Cell Biol. *13*, 989–995.

Pitaval, A., Tseng, Q., Bornens, M., and Théry, M. (2010). Cell shape and contractility regulate ciliogenesis in cell cycle-arrested cells. J. Cell Biol. *191*, 303–312.

Rakic, P. (1972). Mode of cell migration to the superficial layers of fetal monkey neocortex. J. Comp. Neurol. *145*, 61–83.

Ríos, R.M., Sanchís, A., Tassin, A.M., Fedriani, C., and Bornens, M. (2004). GMAP-210 recruits gamma-tubulin complexes to cis-Golgi membranes and is required for Golgi ribbon formation. Cell *118*, 323–335.

Rivas, R.J., and Hatten, M.E. (1995). Motility and cytoskeletal organization of migrating cerebellar granule neurons. J. Neurosci. *15*, 981–989.

Rosenbaum, J.L., and Witman, G.B. (2002). Intraflagellar transport. Nat. Rev. Mol. Cell Biol. *3*, 813–825.

Sánchez-Camacho, C., and Bovolenta, P. (2009). Emerging mechanisms in morphogen-mediated axon guidance. Bioessays *31*, 1013–1025.

Schaar, B.T., and McConnell, S.K. (2005). Cytoskeletal coordination during neuronal migration. Proc. Natl. Acad. Sci. USA *102*, 13652–13657.

Schneider, L., Cammer, M., Lehman, J., Nielsen, S.K., Guerra, C.F., Veland, I.R., Stock, C., Hoffmann, E.K., Yoder, B.K., Schwab, A., et al. (2010). Directional cell migration and chemotaxis in wound healing response to PDGF-AA are coordinated by the primary cilium in fibroblasts. Cell. Physiol. Biochem. *25*, 279–292.

Sedmak, T., and Wolfrum, U. (2010). Intraflagellar transport molecules in ciliary and nonciliary cells of the retina. J. Cell Biol. *189*, 171–186.

Solecki, D.J., Model, L., Gaetz, J., Kapoor, T.M., and Hatten, M.E. (2004). Par6alpha signaling controls glial-guided neuronal migration. Nat. Neurosci. *7*, 1195–1203.

Sorokin, S. (1962). Centrioles and the formation of rudimentary cilia by fibroblasts and smooth muscle cells. J. Cell Biol. *15*, 363–377.

Spassky, N., Han, Y.G., Aguilar, A., Strehl, L., Besse, L., Laclef, C., Ros, M.R., Garcia-Verdugo, J.M., and Alvarez-Buylla, A. (2008). Primary cilia are required for cerebellar development and Shh-dependent expansion of progenitor pool. Dev. Biol. *317*, 246–259.

Stottmann, R.W., Tran, P.V., Turbe-Doan, A., and Beier, D.R. (2009). Ttc21b is required to restrict sonic hedgehog activity in the developing mouse forebrain. Dev. Biol. *335*, 166–178.

Stumm, R.K., Zhou, C., Ara, T., Lazarini, F., Dubois-Dalcq, M., Nagasawa, T., Höllt, V., and Schulz, S. (2003). CXCR4 regulates interneuron migration in the developing neocortex. J. Neurosci. *23*, 5123–5130.

Takahashi, M., Shibata, H., Shimakawa, M., Miyamoto, M., Mukai, H., and Ono, Y. (1999). Characterization of a novel giant scaffolding protein, CG-NAP, that anchors multiple signaling enzymes to centrosome and the golgi apparatus. J. Biol. Chem. *274*, 17267–17274.

Tanaka, D., Nakaya, Y., Yanagawa, Y., Obata, K., and Murakami, F. (2003). Multimodal tangential migration of neocortical GABAergic neurons independent of GPI-anchored proteins. Development *130*, 5803–5813.

Tobin, J.L., Di Franco, M., Eichers, E., May-Simera, H., Garcia, M., Yan, J., Quinlan, R., Justice, M.J., Hennekam, R.C., Briscoe, J., et al. (2008). Inhibition of neural crest migration underlies craniofacial dysmorphology and Hirschsprung's disease in Bardet-Biedl syndrome. Proc. Natl. Acad. Sci. USA *105*, 6714–6719.

Tsai, J.W., Bremner, K.H., and Vallee, R.B. (2007). Dual subcellular roles for LIS1 and dynein in radial neuronal migration in live brain tissue. Nat. Neurosci. *10*, 970–979.

Ueda, M., Gräf, R., MacWilliams, H.K., Schliwa, M., and Euteneuer, U. (1997). Centrosome positioning and directionality of cell movements. Proc. Natl. Acad. Sci. USA *94*, 9674–9678.

Umeshima, H., Hirano, T., and Kengaku, M. (2007). Microtubule-based nuclear movement occurs independently of centrosome positioning in migrating neurons. Proc. Natl. Acad. Sci. USA *104*, 16182–16187.

Willaredt, M.A., Hasenpusch-Theil, K., Gardner, H.A., Kitanovic, I., Hirschfeld-Warneken, V.C., Gojak, C.P., Gorgas, K., Bradford, C.L., Spatz, J., Wölfl, S., et al. (2008). A crucial role for primary cilia in cortical morphogenesis. J. Neurosci. *28*, 12887–12900.

Xu, Q., Wonders, C.P., and Anderson, S.A. (2005). Sonic hedgehog maintains the identity of cortical interneuron progenitors in the ventral telencephalon. Development *132*, 4987–4998.

Xu, Q., Guo, L., Moore, H., Waclaw, R.R., Campbell, K., and Anderson, S.A. (2010). Sonic hedgehog signaling confers ventral telencephalic progenitors with distinct cortical interneuron fates. Neuron *65*, 328–340.

Yokota, Y., Gashghaei, H.T., Han, C., Watson, H., Campbell, K.J., and Anton, E.S. (2007). Radial glial dependent and independent dynamics of interneuronal migration in the developing cerebral cortex. PLoS ONE *2*, e794.